Cell PRESS
Neuron
Article

Lateral Sharpening of Cortical Frequency Tuning by Approximately Balanced Inhibition

Guangying K. Wu,[1,4,5] Robert Arbuckle,[1,5,6] Bao-hua Liu,[1,2] Huizhong W. Tao,[1,3] and Li I. Zhang[1,2,*]
[1]Zilkha Neurogenetic Institute
[2]Department of Physiology and Biophysics
[3]Department of Ophthalmology
[4]Neuroscience Graduate Program
Keck School of Medicine, University of Southern California, 1501 San Pablo Street, Los Angeles, CA 90033, USA
[5]These authors contributed equally to this work.
[6]Present address: Department of Child and Adolescent Psychiatry, School of Medicine, New York University, 550 First Avenue, New York, NY 10016, USA.
*Correspondence: liizhang@usc.edu
DOI 10.1016/j.neuron.2008.01.035

SUMMARY

Cortical inhibition plays an important role in shaping neuronal processing. The underlying synaptic mechanisms remain controversial. Here, in vivo whole-cell recordings from neurons in the rat primary auditory cortex revealed that the frequency tuning curve of inhibitory input was broader than that of excitatory input. This results in relatively stronger inhibition in frequency domains flanking the preferred frequencies of the cell and a significant sharpening of the frequency tuning of membrane responses. The less selective inhibition can be attributed to a broader bandwidth and lower threshold of spike tonal receptive field of fast-spike inhibitory neurons than nearby excitatory neurons, although both types of neurons receive similar ranges of excitatory input and are organized into the same tonotopic map. Thus, the balance between excitation and inhibition is only approximate, and intracortical inhibition with high sensitivity and low selectivity can laterally sharpen the frequency tuning of neurons, ensuring their highly selective representation.

INTRODUCTION

Cortical inhibition plays an important role in shaping receptive field properties of neurons in sensory cortices (Sillito, 1977, 1979; Kyriazi et al., 1996; Wang et al., 2002). The underlying synaptic mechanisms remain controversial. This is partially due to technical limitations, which make it difficult to characterize the structure of cortical inhibitory circuits and the functional properties of cortical inhibitory neurons. The recent application of in vivo whole-cell voltage-clamp recording in the cortex provides a powerful approach to unraveling excitatory and inhibitory synaptic input circuits underlying functions of cortical neurons. In the auditory cortex, two apparently conflicting models have been proposed for inhibitory sharpening of cortical tonal receptive fields (TRFs). First, recent in vivo whole-cell voltage-clamp recordings from individual auditory cortical neurons indicate that the frequency preferences as well as the responding frequency ranges are similar for tone-evoked excitatory and inhibitory synaptic input. This suggests a synaptic input network with balanced excitation and inhibition (Zhang et al., 2003; Wehr and Zador, 2003; Tan et al., 2004; Wu et al., 2006). Because inhibitory input always follows excitatory input with a brief temporal delay, it is proposed that inhibitory input can scale down excitation and thus narrow the frequency range for spike responses in a so-called "iceberg" effect (Wehr and Zador, 2003). Second, it was proposed previously that cortical inhibitory input may have broader tuning than excitatory input, resulting in lateral inhibition in the surround of TRFs (Suga and Manabe, 1982; Shamma, 1985; Calford and Semple, 1995; Sutter and Loftus, 2003; Oswald et al., 2006). This second model is primarily based on extracellular recording experiments of two-tone suppression, in which one tone modifies (usually suppresses) the response to a later tone (Suga and Manabe, 1982; Calford and Semple, 1995; Sutter and Loftus, 2003). Although the response properties of auditory cortical inhibitory neurons are largely unknown, several extracellular studies in the somatosensory cortex suggest that putative cortical inhibitory neurons may possess less selective representational properties than principal neurons (Simons and Carvell, 1989; Swadlow, 1989), supporting the second model.

In previous intracellular studies (Wehr and Zador, 2003; Zhang et al., 2003; Tan et al., 2004), the patterns of tone-evoked excitatory and inhibitory inputs have not been examined in sufficient detail. Although inhibitory input has been shown to be able to scale down the level of membrane excitation, no direct comparison has been made between the frequency tuning curves of membrane potential responses in the presence and absence of inhibition. Thus, the existence of lateral inhibitory effects cannot be excluded by the findings on the apparently balanced excitation and inhibition. In this study, we tested the possibility that tone-evoked synaptic excitation and inhibition in a single cortical neuron do not match precisely and that the fine structure in their distribution patterns can result in an equivalent lateral inhibitory sharpening of TRFs.

Studies on the pattern of inhibitory input to a cortical neuron alone cannot fully address the response properties of presynaptic inhibitory neurons, except that the spike TRFs of the presynaptic inhibitory neurons will be no larger than the tonal responsive area defined by the inhibitory inputs to the cell. Because only 15%–25% of neurons are inhibitory in many cortical areas (Peters and Kara, 1985; Hendry et al., 1987; Priet et al., 1994) and it remains difficult to identify and target these neurons in vivo, our knowledge of their functional properties has lagged far behind that of excitatory neurons. There have been limited studies on the functional properties of cortical inhibitory neurons. In the rabbit somatosensory cortex, extracellular recordings from suspected inhibitory neurons (SINs), identified according to their spike features, suggest that SINs lack directional preference, unlike principal cells, and exhibit high sensitivity to sensory stimuli (Swadlow, 2003). In the cat visual cortex, pioneering studies with intracellular recording and biocytin labeling have reported both simple and complex-cell-like inhibitory neurons, with their orientation tuning properties ranging from unselective to tightly tuned (Azouz et al., 1997; Hirsch et al., 2003). By using Ca^{2+} imaging, a recent study in superficial layers of mouse visual cortex suggests that GABAergic neurons exhibit much weaker orientation selectivity compared to non-GABAergic neurons (Sohya et al., 2007). Despite limited studies in visual and somatosensory cortices, functional properties of inhibitory neurons in auditory cortex have rarely been examined. Because the sampling bias in the classic "blind" whole-cell recording method (which prefers larger cells such as pyramidal) and the sparse distribution of inhibitory neurons prevent effective sampling of these neurons, in this study, we combined cell-attached recording with juxtacellular labeling or subsequent intracellular recording to selectively target fast-spike inhibitory neurons, the major source of local inhibitory input to pyramidal neurons. Our results suggest that fast-spike inhibitory neurons exhibit broader frequency tuning than excitatory neurons, and this property may contribute to the equivalent lateral-inhibition effect.

RESULTS

Frequency Tuning Curves of Excitatory and Inhibitory Inputs

To examine fine structures in the spectral patterns of excitatory and inhibitory input to auditory cortical neurons, we applied blind in vivo whole-cell voltage-clamp recordings in the recipient layer (layer 4) of the rat primary auditory cortex (A1). The blind whole-cell recording method used under our experimental conditions resulted in recording exclusively from excitatory neurons, as described previously (Wu et al., 2006). The auditory stimuli were pure tones of various frequencies and intensities, which were presented in a pseudorandom sequence. Excitatory and inhibitory synaptic currents in response to tones were recorded under the clamping voltages of −70 mV and 0 mV, respectively, the potential levels close to the reversal potential for $GABA_A$ receptor and glutamate receptor-mediated currents, respectively. The excitatory and inhibitory synaptic conductances were derived from synaptic currents (see Experimental Procedures). As shown by an example cell in Figures 1A and 1B, the excitatory and inhibitory synaptic TRFs largely overlap with each other, consistent with previous reports (Zhang et al., 2003; Tan et al., 2004; Wu et al., 2006). Interestingly, after deriving the envelope of response peaks, i.e., the frequency tuning curve, for both excitatory and inhibitory synaptic input at 70 dB sound pressure level (SPL), we observed that the inhibitory frequency tuning curve was more flattened than that of excitatory input, as reflected by the faster saturation of conductance magnitude along the frequency domain and the more plateau-like peak of the tuning curve (Figure 1C). To quantify this effect, we measured the bandwidth of the tuning curve at 60% of maximum value (60% BW) for both excitatory and inhibitory input. At all test intensities above the subthreshold intensity threshold (20 dB in this cell), the 60% BWs of inhibitory input (Figure 1D, red lines) were consistently broader than those of excitatory input (Figure 1D, black lines), suggesting that inhibitory input is less selectively tuned.

The less selective inhibitory tuning will presumably generate relatively more inhibition in frequency regions flanking the peak of the excitatory tuning curve and result in a narrowing of frequency tuning in a manner analogous to lateral inhibition. To demonstrate this effect, we derived tone-evoked membrane potential changes for the same cell with and without considering inhibitory input (see Experimental Procedures). As shown in Figure 1E, the tuning curve of derived membrane potential responses at 70 dB SPL was sharper when excitatory and inhibitory input were integrated than when only excitatory input was considered. The relative sharpening effect of inhibition was demonstrated by subtracting the normalized membrane potential tuning curve derived without considering inhibition from that when inhibition was present (Figure 1E, blue). Apparently stronger inhibitory effect is generated at the flanks of the peak of membrane excitation, which determines the best frequency of the cell (Figure 1E).

Lateral Inhibitory Sharpening of Frequency Tuning

For the other ten cells in which both excitatory and inhibitory currents were recorded, we derived the excitatory and inhibitory frequency tuning curves (Figures 2A and 2B), as well as the tuning curves of membrane potential changes in the absence and presence of inhibition (Figure 2C). In all of these cells, the inhibitory tuning curve exhibited broader bandwidths than the excitatory tuning curve around its peak, although the responding frequency range of inhibitory input was similar to or slightly narrower than that of excitatory input (Figure 2B). In result, the derived membrane potential tuning curves in the presence of inhibition were narrower around the peak than those in the absence of inhibition (Figure 2C). By comparing the two normalized membrane potential tuning curves for each cell, we estimated the relative suppression effect of inhibition at different tone frequencies. In all of the cases, suppression tended to increase from the center of the best frequency on both sides, consistent with the concept of lateral inhibition or inhibitory sidebands.

The percentage difference in the bandwidth of excitatory and inhibitory tuning curves at various levels were summarized for all 11 cells (Figure 3). We found that the responding frequency range (i.e., 0%BW) of inhibitory input was on average slightly narrower than that of excitatory input (Figure 3A). In contrast, inhibitory tuning curve was significantly broader at the levels of 40%, 60%, and 80% of maximum amplitude (Figure 3A). This was

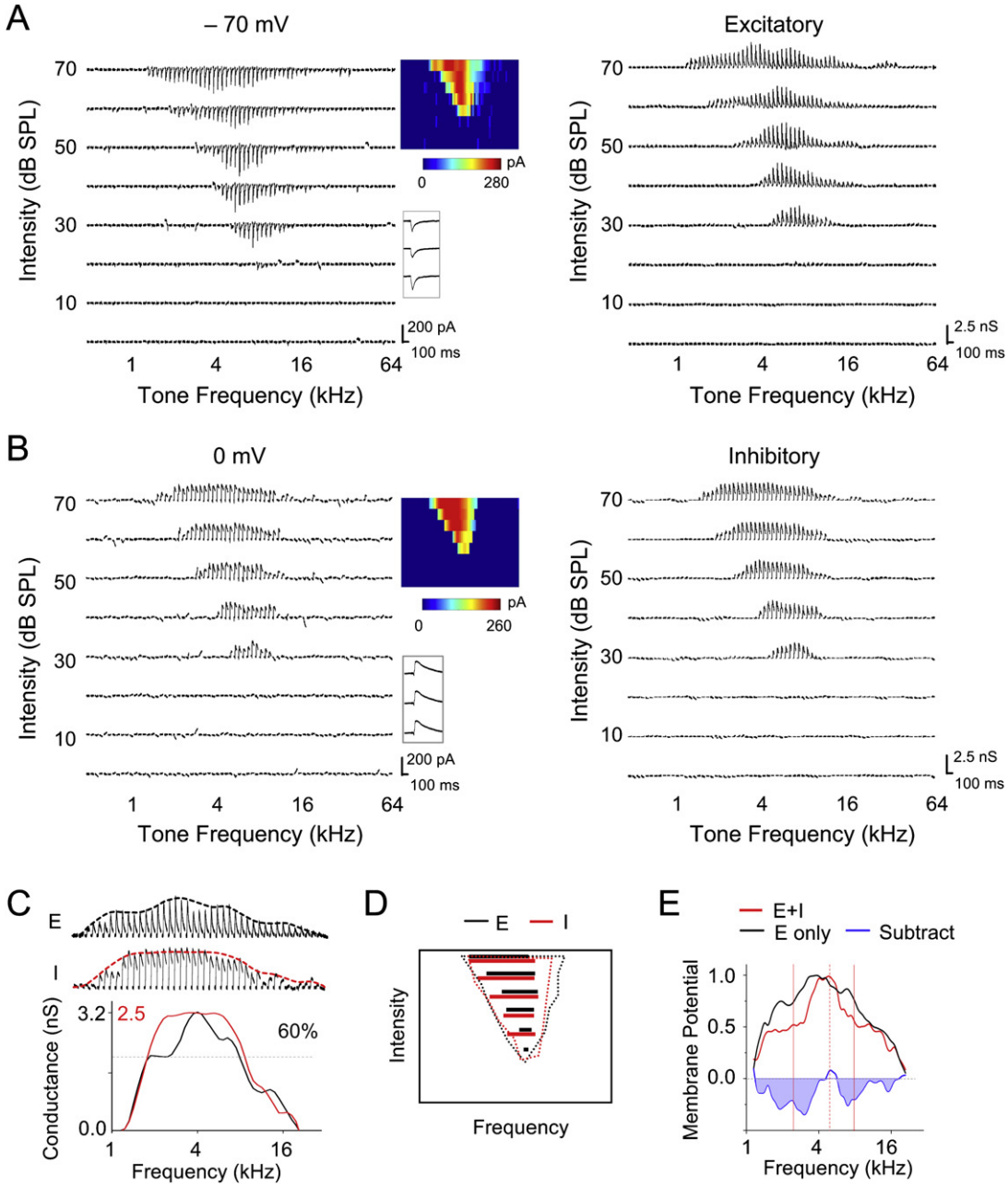

Figure 1. Frequency Tuning of Synaptic Inputs in an Example A1 Excitatory Neuron

(A and B) (Left) Excitatory (A) and inhibitory (B) synaptic currents recorded in an example neuron at −70 mV and 0 mV, respectively, in response to pure tones of various frequencies and intensities. Each small trace represents a response to a tone (averaged from two repeats). (Middle) Color maps represent the TRFs of synaptic responses, with the color of each pixel indicating the peak amplitude of synaptic currents. Inset below the color map shows individual traces (250 ms) of synaptic currents responding to a best-frequency tone at 40, 50, and 60 dB sound pressure level (SPL). (Right) TRFs of excitatory and inhibitory synaptic conductances, which were derived from the averaged synaptic currents.

(C) The enlarged profile of excitatory (upper) and inhibitory (middle) conductances at 70 dB SPL for the same cell (cell1). Envelopes, i.e., frequency tuning curves, were calculated from the peak amplitudes of synaptic conductances and were indicated by the dashed lines. (Bottom) The inhibitory tuning curve was superimposed with the excitatory curve. The black and red scale values are for the excitatory and inhibitory curve, respectively.

(D) Dotted lines depict the boundary of TRFs of excitatory (black) and inhibitory (red) input for the same cell. Colored solid lines indicate the frequency ranges for responses with amplitudes larger than 60% of maximum value at each testing intensity. Black, excitatory; red, inhibitory.

(E) Frequency tuning curve of derived peak membrane potential responses when only excitatory input was considered (black) or when both excitatory and inhibitory inputs were considered (red). The tuning curves are normalized. The subtraction between the two curves is shown by the blue line. Dashed red vertical line indicates the frequency for the peak response, and the two solid red vertical lines indicate the estimated frequency range of spike responses.

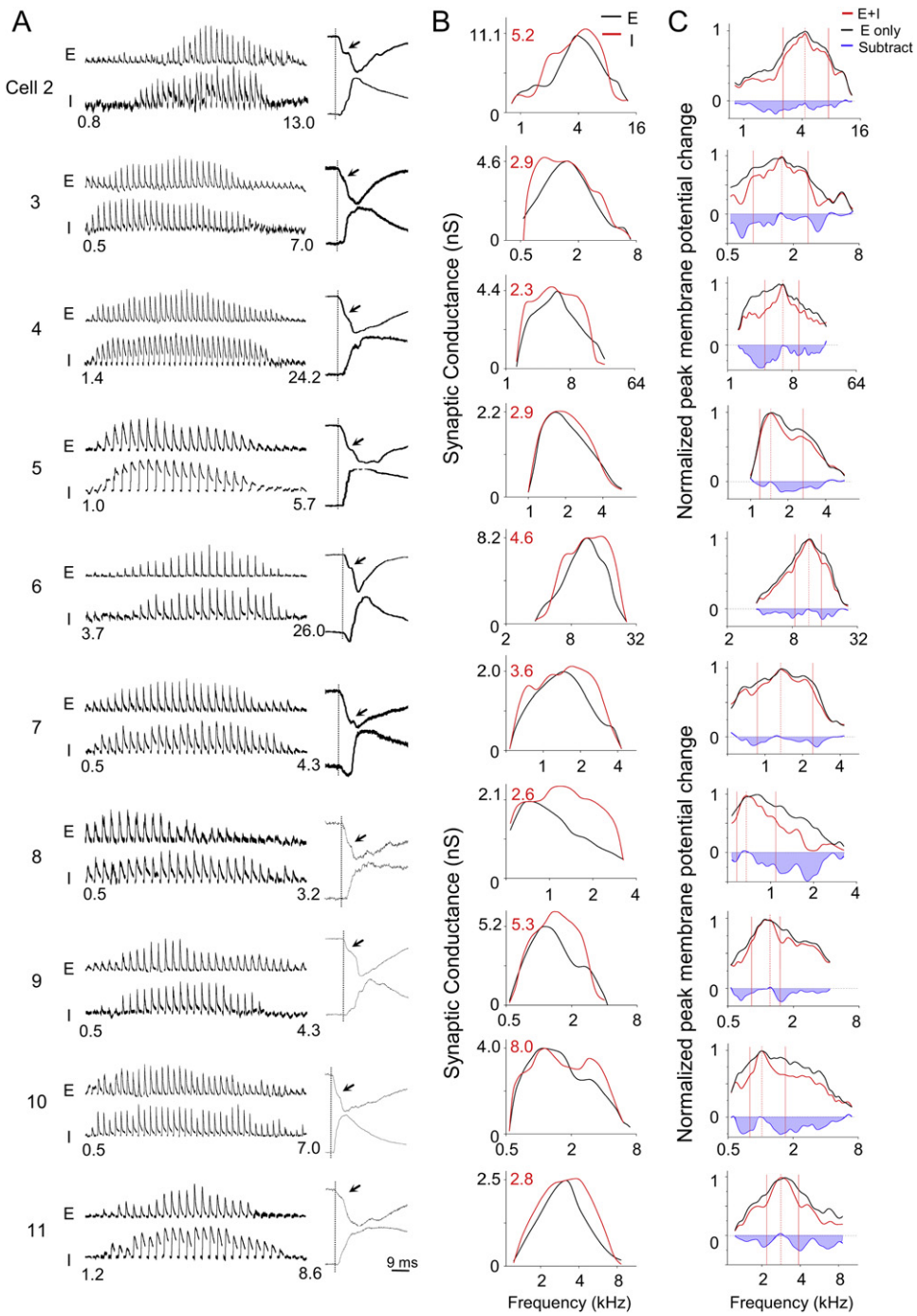

Figure 2. Frequency Tunings of Synaptic Inputs in Ten Other Excitatory Neurons in A1

(A) (Left) Derived excitatory ("E") and inhibitory ("I") synaptic conductances within the responding frequency range (labeled by numbers below) at 70 dB SPL. (Right) Example traces of excitatory (upper) and inhibitory responses (lower) to a best-frequency tone. Traces are normalized to have the same peak amplitude. Vertical line indicates the onset of excitatory response. Arrowheads indicate that excitatory currents normally exhibit two phases in their arising kinetics. The onsets of inhibitory inputs are roughly at the transition between these two phases.

(B) Tuning curves of excitatory (black) and inhibitory (red) conductances were superimposed for comparing their shapes. The black and red scale values are for excitatory and inhibitory curves, respectively.

(C) Normalized tuning curves of membrane potential changes derived for the cells shown in (A) and (B), with (red) and without (black) considering inhibition. Data are presented in a similar manner as in Figure 1E.

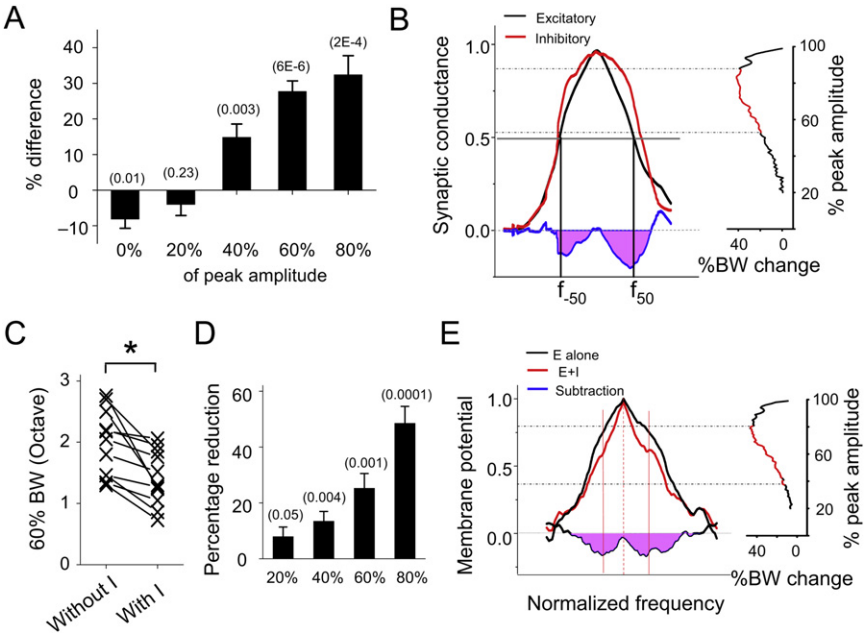

Figure 3. Summary of Frequency Tunings of Synaptic Inputs and Membrane Potential Responses

(A) Average percentage difference in bandwidth between excitatory and inhibitory tuning curves ((In − Ex)/In) at different amplitude levels. Data are from the 11 cells shown in Figures 1 and 2. Bar represents SEM. The numbers in the parenthesis indicate the "p" values for the statistics (paired t test, n = 11).

(B) (Left) Average frequency tuning curve of excitatory (black) and inhibitory (red) conductances after normalization (see Experimental Procedures). f_{-50} and f_{50} are two reference points for aligning normalized tuning curves. (Right) Percentage difference in bandwidth between the two averaged tuning curves at different amplitude levels (step size = 1%). Data point labeled with red color indicates significant difference ($p < 0.05$; two-way ANOVA).

(C) Bandwidths of membrane potential tuning curves without and with inhibition at 60% of maximum amplitude (60% BW). *, paired t test, $p < 0.0001$, n = 11 cells.

(D) Percentage reduction in bandwidth of membrane potential tuning curves after integration of inhibition at the levels of 20%, 40%, 60%, and 80% of maximum response, summarized for the 11 cells. Bar = SEM. "p" values are indicated in the parenthesis (one-group t test, n = 11).

(E) (Left) Average frequency tuning curve of peak membrane potential changes with (red) or without inhibition (black). Blue line is plotted similarly as that in Figure 1E. Solid red vertical lines indicate the estimated spiking frequency range. (Right) Percentage reduction in bandwidth along the tuning curves (1% step) after integrating inhibition, analyzed in the same way as in (B).

further demonstrated by averaging all the normalized synaptic tuning curves (Figure 3B; see Experimental Procedures). The broader inhibitory bandwidths at the flanks of the excitatory tuning peak can result in relatively stronger inhibition around the excitation peak, as shown by the subtraction of the two averaged tuning curves. By examining the bandwidths at all levels (at 1% step), we found that between the levels of 54% and 88% of maximum amplitude the bandwidths of the average inhibitory tuning curve were significantly broader than those of the excitatory tuning curve (n = 11, two-way ANOVA, $p < 0.05$).

The effect of inhibition on the membrane potential tuning curve was quantified by comparing the tuning curves of membrane potential responses generated with and without inhibitory inputs. In the presence of inhibition, the bandwidths of tuning curves were significantly reduced at various levels (e.g., 40%, 60%, and 80% of maximum amplitude) (Figures 3C and 3D). The percentage reduction in bandwidth appeared to increase as the measurement moved closer to the peak of membrane response tuning curve (Figure 3D). To further demonstrate this effect, the membrane potential tuning curves generated with and without inhibition were normalized (in both amplitude and frequency domains) for all the cells and then were averaged (Figure 3E; see Experimental Procedures). There was a significant reduction in bandwidth due to inhibition between the levels of 40% and 78% of peak response (Figure 3E, right). The greatest reduction appears at the level rather close to the peak (Figure 3E, right). Here, we also estimated the spike response range in the averaged membrane potential tuning curve, since the spike threshold was at the level of about 60% of maximum response (Figure 2C; 59.6% ± 5.8%, mean ± SD, n = 11; see Experimental Procedures). Within the estimated frequency range of spike responses, the relative suppression increased from the peak of the tuning curves on both sides. Together, these results demonstrate that the balance of excitation and inhibition is only approximate and that, in addition to generally reducing excitation, the more broadly tuned inhibitory input can further sharpen the frequency representation of cortical neurons by laterally narrowing the tuning curve especially at around the excitation peak.

Fast-Spike Inhibitory Neurons and Regular-Spike Excitatory Neurons

Why does inhibitory input exhibit less selective frequency tuning than excitatory input? Our recent study suggests that the shape of membrane potential tuning curve (especially in the suprathreshold frequency ranges) is largely defined by recurrent cortical excitatory inputs (Liu et al., 2007). Thus, if cortical inhibitory neurons have broader frequency tuning than cortical excitatory neurons, this can cause broader tuning of inhibitory input. Previous studies in cortical slices demonstrate that cortical pyramidal neurons in the input layer primarily receive inhibitory input from nearby fast-spike inhibitory neurons (Agmon and Connors, 1992; Gil and Amitai, 1996; Gibson et al.,1999; Inoue and Imoto, 2006; Sun et al., 2006). To examine the frequency tuning and spike TRF of inhibitory neurons, we applied cell-attached recording and juxtacellular labeling (see Experimental Procedures) to distinguish neuronal types according to the spiking property and morphology of the recorded cells. With cell-attached recording, only spikes from the targeted neuron are recorded. Because the pipette capacitance was completely compensated in our experiments, distortion of spike waveform was minimized,

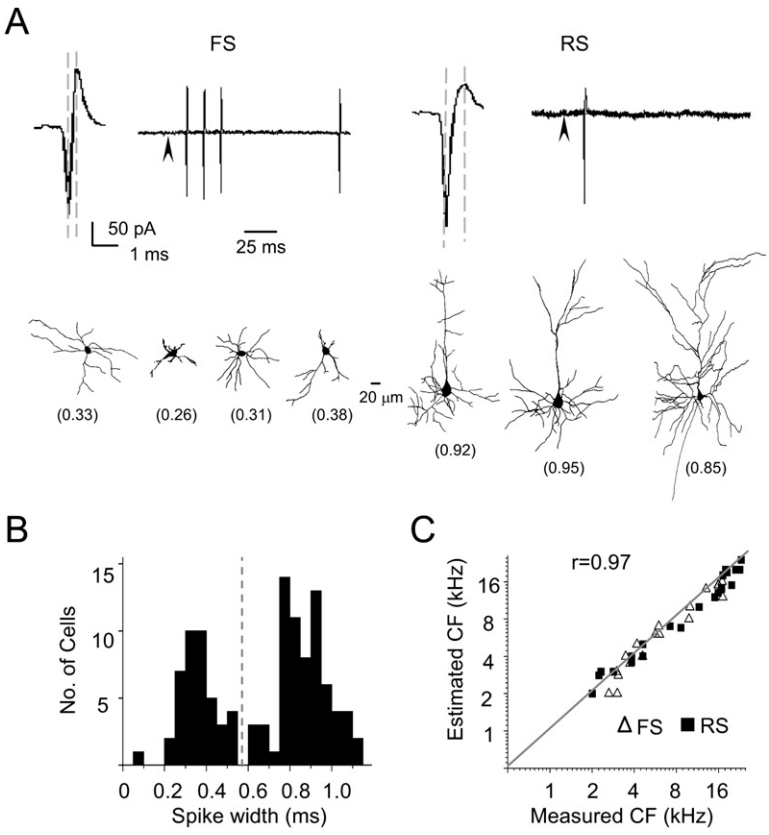

Figure 4. Cell-Attached Recordings from Fast-Spike and Regular-Spike Neurons and Juxtacellular Labeling

(A) (Upper panel) Example spike waveform and tone-evoked spike response in an FS (left) and an RS neuron (right). Two dashed lines indicate the peak-to-peak interval. Arrowhead indicates the onset of tone stimulus. (Lower panel) Example reconstructed dendritic morphologies of neurons labeled by juxtacellular methods following cell-attached recordings. The values of their peak-to-peak intervals (ms) are indicated in the parenthesis.

(B) Distribution of average peak-to-peak intervals from 111 recorded cells. The dashed line indicates the separation between the groups of FS and RS neurons in this study. Sampling here was not random because we specifically searched for fast-spike neurons.

(C) Correlation between the CFs of neurons determined from their spike TRFs and the CFs predicted from their positions in the tonotopic map, which was determined with multiunit extracellular recordings.

and thus we could compare the spike waveforms from different recordings. Figure 4A (upper panel) shows two typical types of spikes, either spontaneously generated or evoked by tone stimuli. The first type (observed in about 10% of encountered neurons; see Experimental Procedures) exhibits a relatively large upward peak and a short peak-to-peak interval, which is defined as the time interval between the trough and the upward peak of the spike waveform. The second type has a smaller upward peak and a longer peak-to-peak interval. According to the distribution of peak-to-peak intervals (Figure 4B), we arbitrarily categorized the recorded neurons into two groups: fast-spike (FS, with peak-to-peak interval <0.6 ms) and regular-spike (RS, with peak-to-peak interval $\geq$0.6 ms) neurons. The average peak-to-peak interval is 0.35 ± 0.09 ms (mean ± SD; n = 42) for fast-spike neurons and 0.83 ± 0.12 ms (n = 69) for regular-spike neurons. The spiking property of FS neurons is consistent with previous reports of fast-spiking inhibitory neurons (Mountcastle et al., 1969; Swadlow, 1989; Azouz et al., 1997). The fast-spike neurons often exhibit a train of action potentials when stimulated with a brief tone, while regular-spike neurons usually exhibit single-spike responses (Figure 4A). Based on the morphology of the recorded cells successfully reconstructed after juxtacellular labeling or intracellular labeling (see Experimental Procedures), we found that the fast-spike neurons exhibited locally constrained and smooth dendritic arbors, while typical pyramidal-cell morphology with spiny dendritic arbors were mostly observed for regular-spike neurons (Figure 4A, lower panel). Previous studies have shown that fast-spiking neurons are parvalbumin-positive GABAergic neurons, occupying about 70% inhibitory neuron population in layer 4 (Kawaguchi and Kubota, 1997; Gonchar and Burkhalter, 1997). It is reasonable to assume that the fast-spike neurons recorded under our condition were inhibitory and that the regular-spike neurons were primarily excitatory. Since the characteristic frequencies (CFs) of the recorded fast-spike and regular-spike neurons correlate equally well with the estimated CFs for these cells (predicted according to their positions in the A1 tonotopic map, see Experimental Procedures), we conclude that inhibitory neurons are organized into the same tonotopic map as excitatory neurons (Figure 4C). The same tonotopic map for both excitatory and inhibitory neurons suggests that the topographic organization of thalamocortical innervation is independent of cortical neuronal types.

Spike TRFs of Fast-Spike Inhibitory Neurons

Because the majority of inhibitory neurons in layer 4 are fast-spike neurons, we specifically examined the spike TRFs of this type of inhibitory neuron. In Figures 5A and 5B, two nearby fast-spike and regular-spike neurons in the same preparation were recorded with the cell-attached recording method. Their complete spike TRFs were reconstructed and compared. The fast-spike neuron was tuned with a CF close to that of the regular-spike neuron (2.8 and 1.9 kHz, respectively, see Experimental Procedures). It appeared that the TRF area of the fast-spike neuron was larger than that of the regular-spike neuron, with a lower intensity threshold and broader responding frequency ranges at all testing intensities. To compare the TRF properties between fast-spike and regular-spike neurons, a group of FS and RS neurons were randomly recorded (see Figures S3 and S4). We arbitrarily divided these cells into two groups according to their CFs (CF < 6 kHz and CF $\geq$ 6 kHz) since TRF properties may also depend on the cell's CF (Zhang et al., 2001; Polley et al., 2007). As shown in Figure 5C and Figure S2, the responding frequency ranges at all testing intensities were significantly

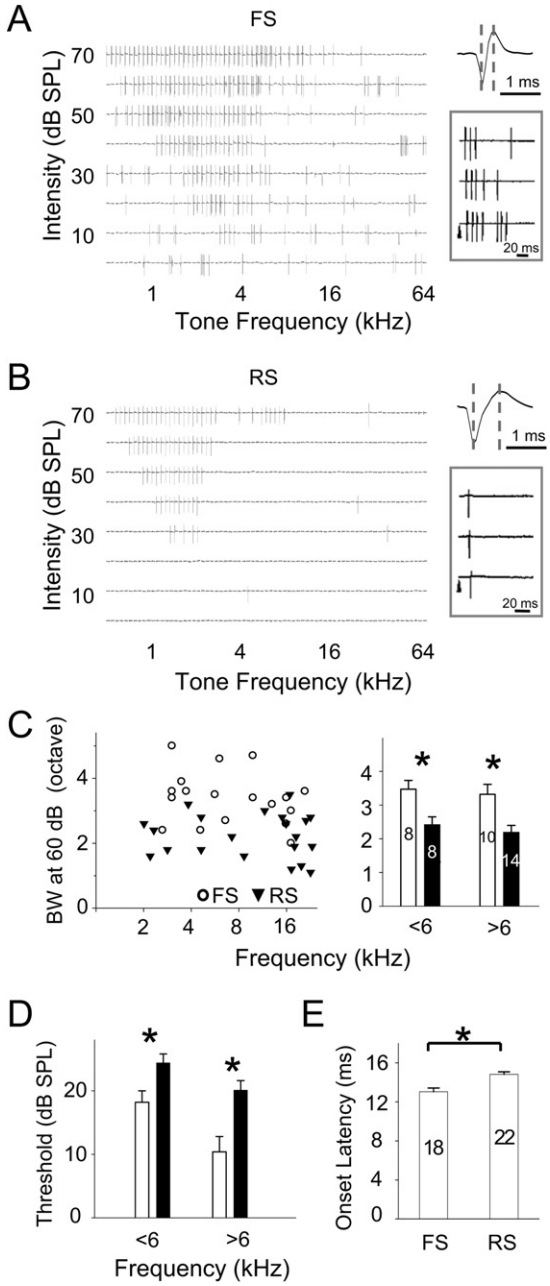

Figure 5. Spike TRFs of FS and RS Neurons

(A and B) Example spike TRF of an FS neuron (A) and a nearby RS neuron (B). The enlarged recording trace indicates the spike waveform (right). Inset shows tone-evoked spikes in single trials. Arrowhead indicates the onset of tone stimulus.

(C) (Left) Distribution of bandwidths of spike TRFs at 60 dB SPL (BW60) plotted against the cells' CFs. (Right) Average spike BW60 of FS (open) and RS (filled) cells with CFs below or above 6 kHz. Bars are SEM. *, two-sample t test, $p < 0.02$.

(D) Average intensity threshold of spike TRFs of the same group of FS (open) and RS (filled) neurons with CFs below or above 6 kHz. Bars are SEM. *, two-sample t test, $p < 0.02$.

(E) Average onset latency of the first tone-evoked spike in FS and RS neurons. Bars are SEM. *, two-sample t test, $p < 0.001$. The number of cells is indicated.

broader in fast-spike neurons, and the intensity threshold of their TRFs was significantly lower than that of regular-spike neurons (Figure 5D). The broader bandwidth and lower intensity threshold predict that the fast-spike neurons possess significantly larger TRFs than nearby regular-spike neurons. In other words, at a given intensity, fast-spike inhibitory neurons exhibit less-selective frequency tuning than nearby excitatory neurons. Neurons in layer 4 receive excitatory input primarily through thalamocortical and local intracortical excitatory projections and receive inhibitory input mainly from local fast-spike neurons. The broader spike TRFs of fast-spike neurons compared to those of nearby excitatory neurons will account, at least partially, for the less-selective frequency tuning of inhibitory input.

TRF of Membrane Potential Responses in Fast-Spike Inhibitory Neurons

We next examined whether the broader TRFs of fast-spike inhibitory neurons are due to broader ranges of their excitatory inputs or to their more efficient conversion of synaptic inputs to spike outputs. Because of the sparse distribution of inhibitory neurons, cell-attached recording followed by whole-cell current-clamp recording was applied to select fast-spike neurons. Their TRFs of membrane depolarization responses were examined (Figure 6A). Here, tone-evoked membrane depolarizations were identified according to the amplitude and onset latency of membrane potential changes following the stimulus onset (see Experimental Procedures). We then compared the spike TRF (determined with initial cell-attached recording) and the TRF of membrane depolarizations (determined with subsequent current-clamp recording) of the same cell. In the fast-spike inhibitory neuron, the spike TRF largely overlapped with the TRF of membrane depolarization responses, with the same intensity threshold and slightly narrower responding frequency ranges above the intensity threshold (Figures 6A and 6C). In comparison, a regular-spike neuron that had a similar CF exhibited a smaller spike TRF, leaving larger subthreshold regions at the periphery of its membrane potential TRF (Figures 6B and 6C). A total of six fast-spike neurons and nine regular-spike neurons were recorded with both spike and membrane potential TRFs obtained. The percentage occupancy of spike response region in the membrane response region was measured at 60 dB SPL (Figure 6D, left). The fast-spike neurons possessed relatively larger spike response regions (77.3% ± 8.5%, mean ± SD, n = 6) than regular-spike neurons (54.3% ± 7.6%, n = 9; two-sample t test, $p < 0.001$). In the meantime, the frequency range of membrane depolarization responses at 60 dB SPL was not significantly different between the two groups of neurons (Figure 6D, right). Thus, our results demonstrate that the frequency range of excitatory inputs is similar between fast-spike and regular-spike neurons. However, fast-spike neurons can convert a broader range of synaptic inputs into spike outputs. This may be partially due to stronger thalamocortical synapses made on fast-spike inhibitory neurons than on pyramidal cells, as suggested by several recent studies in cortical slices (Cruikshank et al., 2007; Daw et al., 2007). Further technical development will be needed to address the synaptic mechanisms underlying the high sensitivity of fast-spike neurons (see Experimental Procedures). Nonetheless, the less-selective outputs from fast-spike neurons may contribute to the more broadly tuned

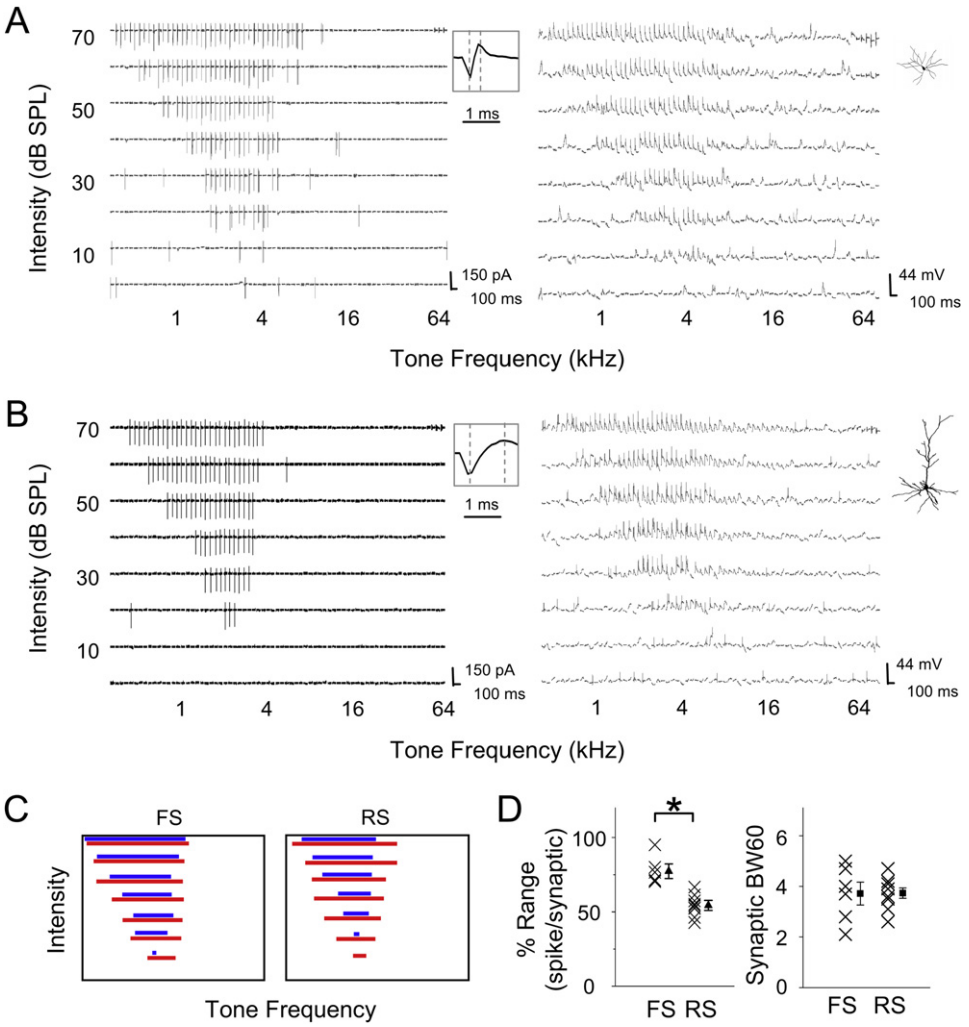

Figure 6. Suprathreshold and Subthreshold Regions of Synaptic TRFs in FS and RS Neurons

(A and B) (Left) Spike TRF of an FS (A) and an RS (B) neuron mapped with cell-attached recordings. Enlarged spike waveform is shown in the inset. (Right) TRF of membrane potential responses mapped with subsequent whole-cell current-clamp recording. Insets show the reconstructed morphology of the recorded FS and RS cells labeled with intracellular loading of biocytin.

(C) (Left) Frequency ranges of synaptic responses (red) and spike responses (blue) at different intensities for cells shown in (A) and (B).

(D) (Left) Percentage frequency range of spike responses relative to synaptic responses at 60 dB SPL in FS (n = 6) and RS neurons (n = 9). Two groups are significantly different ($p < 0.001$, two-sample t test). (Right) Frequency range of synaptic responses at 60 dB SPL in FS and RS neurons. Bar, SEM.

inhibitory input to cortical excitatory neurons and result in the lateral sharpening of frequency representation of these cells.

DISCUSSION

In this study, we examined the detailed patterns of excitatory and inhibitory input to individual cortical excitatory neurons. We have revealed that under approximately balanced excitation and inhibition, inhibitory input exhibits significantly broader frequency tuning than excitatory input. This results in relatively stronger inhibition in frequency regions flanking the preferred frequencies of the cell and an effective lateral sharpening of its frequency tuning. By further examining the spike TRFs of fast-spike inhibitory neurons, our results suggest that the observed lateral sharpening may be attributed to the broader spike TRFs of fast-spike neurons compared to regular-spike neurons. In addition, intracellular recordings indicate that the broader spike TRFs of fast-spike neurons are not due to broader ranges of excitatory inputs to these neurons, but to their higher efficiency of converting inputs to spike outputs.

Approximately Balanced Excitation and Inhibition

Previous in vivo whole-cell recording studies have led to the conclusion that balanced excitation and inhibition underlie the frequency-intensity tonal receptive field in the rat auditory cortex. This is evidenced by the following: first, excitatory and inhibitory synaptic receptive fields are largely matched and exhibit similar preferred frequencies (Zhang et al., 2003; Wehr and

Zador, 2003; Tan et al., 2004; Wu et al., 2006); second, excitatory and inhibitory conductances activated by the same tone stimulus have similar amplitudes and exhibit significant linear covariation under different tone stimuli (Wehr and Zador, 2003; Zhang et al., 2003; Tan et al., 2004); third, inhibition closely follows excitation, resulting in a scaling down of excitation (Ojima and Murakami, 2002; Wehr and Zador, 2003; Tan et al., 2004; Wu et al., 2006). However, the "balance" between excitation and inhibition has not been quantified with sufficient measuring resolutions in previous studies. In this study, our data are largely consistent with the concept of balanced excitation and inhibition in that excitatory and inhibitory inputs have similar TRF areas and preferred frequencies. However, more detailed examination of the tuning patterns of excitatory and inhibitory inputs reveals that the balance is in fact only approximate. Inhibition has less-selective frequency tuning than excitation, as reflected by the broader 60% BW and 80% BW, which contribute significantly to the spike frequency range of the cell. Our analysis further suggests that under the approximate balance, the fine structures in the excitatory and inhibitory tuning patterns can endow extra processing power to cortical neurons.

Inhibitory Mechanisms for Shaping Frequency Representation

Previous pharmacological experiments in sensory cortices have shown that blocking cortical inhibition results in a reduction of representational selectivity, e.g., orientation selectivity in the visual cortex (Sillito, 1977, 1979; Crook et al., 1997) and frequency selectivity in the auditory cortex (Chen and Jen, 2000; Wang et al., 2000, 2002). Previous studies have demonstrated that synaptic inhibition closely follows the excitation evoked by the same tone stimulus and can interact with excitation to shape the spike response. In our work, the onset of inhibitory input was found to be 2.7 ± 0.5 ms (mean ± SD, n = 15 neurons; evoked by CF tones at 70 dB) after that of excitatory input, while the onset of the first tone-evoked spike was 4.5 ± 0.8 ms (n = 8 neurons; obtained in current-clamp recordings) after that of excitatory input (also see Figure 5E). The significant later onset of the first spike compared to that of inhibitory input (independent t test, $p < 0.001$) indicates that inhibitory input can affect spike responses. This is consistent with previous findings in the thalamocortical circuit of various sensory cortices that show that the temporally delayed inhibitory input can control the threshold for the generation of spike responses (e.g., Douglas and Martin 1991; Somers et al., 1995; Anderson et al., 2000; Zhang et al., 2003; Wehr and Zador, 2003; Tan et al., 2004; Higley and Contreras, 2006). Because inhibition is roughly balanced with excitation in the rat auditory cortex, it is proposed that the inhibitory sharpening of frequency tuning can be simply achieved through generally scaling down the level of excitation (Wehr and Zador, 2003; Tan, et al., 2004). In this study, our data have revealed an additional mechanism for inhibitory sharpening, i.e., an equivalent lateral inhibitory effect. Since inhibitory tuning curve exhibits a broader peak than excitation, it generates relatively stronger inhibition in frequency regions at the flanks of the excitation peak and thus narrows the tuning curve of membrane potential responses round the peak. Taken together, our results have united the two models of balanced excitation-inhibition and lateral inhibition and demonstrate that fine structures in the pattern of synaptic inputs can play significant roles in determining cortical representation and processing functions.

Properties of Auditory Cortical Inhibitory Neurons

In many cortical areas, only 15%–25% of total neurons are GABAergic inhibitory neurons (Peters and Kara, 1985; Hendry et al., 1987; Priet et al., 1994). Because of their sparseness and the difficulty in identifying them in vivo, our knowledge of functional properties of cortical inhibitory neurons is scarce; neither do we know much about the structure of inhibitory circuits. Extracellular recordings from suspected inhibitory neurons in the input layer of rabbit somatosensory cortex suggest that they respond unselectively to the direction of whisker displacement, while principal cells are known to exhibit direction selectivity (Swadlow, 2003). In layer 4 of cat primary visual cortex, two functional populations of inhibitory cells (simple and complex, similar to pyramidal neurons) were identified by intracellular recording and biocytin labeling (Hirsch et al., 2003), while a recent calcium imaging study in mice suggests that, in layer 2/3, GABAergic neurons exhibit much weaker orientation selectivity compared to non-GABAergic neurons (Sohya et al., 2007). There are different subtypes of inhibitory neurons according to their distinct physiological, morphological, and neurochemical properties (Kawaguchi and Kubota, 1997; Gonchar and Burkhalter, 1997; Gupta et al., 2000). In this study, by combining cell-attached spike recording with juxtacellular labeling or with subsequent whole-cell recording and labeling, we specifically targeted fast-spike inhibitory neurons in the rat A1. Fast-spike inhibitory neurons are parvalbumin positive and occupy about 70% of the inhibitory neuron population in layer 4. The major type of fast-spike neurons is basket cells. The minor type is chandelier cells, which normally are not driven by sensory inputs under physiological conditions (Zhu et al., 2004). Thus, tone-evoked inhibitory inputs to layer 4 neurons are likely provided primarily by nearby fast-spike basket cells. Our results indicate that fast-spike inhibitory neurons have broader spike TRFs and exhibit lower selectivity but higher sensitivity in response to tonal stimuli, consistent with the conventionally assumed role of cortical inhibitory neurons.

Implication on Cortical Circuitry

The onsets of tone-evoked spike responses in fast-spike inhibitory neurons are slightly earlier (13.05 ± 0.37 ms, mean ± SEM, n = 18) than those of regular-spike neurons (14.82 ± 0.26 ms, n = 22; Figure 5E). Because fast-spike inhibitory neurons are the major source of cortical inhibition in layer 4 (Agmon and Connors, 1992; Gil and Amitai, 1996; Gibson et al.,1999; Inoue and Imoto, 2006; Sun et al., 2006), this suggests that inhibitory inputs to layer 4 neurons could be primarily feedforward (Tan et al., 2004). In addition, our data indicate that neighboring fast-spike and excitatory neurons have similar preferred frequencies and frequency ranges of excitatory inputs (as indicated by the tone-evoked membrane depolarizations). Thus, a simplified circuitry model can be proposed here: the neighboring excitatory neurons and fast-spike inhibitory neurons are innervated by a similar set of thalamocortical axons, and the excitatory neurons also receive feedforward inhibition from the fast-spike neurons. The slightly narrower frequency range of inhibitory input

compared to that of excitatory input in pyramidal neurons (Figure 3A) can be attributed to the fact that the frequency range of spike output of fast-spike neurons is slightly narrower than that of their excitatory input (Figures 6C and 6D). Because the amplitudes of inhibitory inputs are graded at any given testing intensity, the recorded pyramidal neuron likely receives inhibitory inputs from a group of cortical inhibitory neurons. Further understanding of the distribution pattern of inhibitory neurons that project to a single pyramidal neuron will be needed for a more realistic model of cortical inhibitory circuitry.

EXPERIMENTAL PROCEDURES

Animal Preparation and Extracellular Recording

All experimental procedures used in this study were approved under the Animal Care and Use Committee at the University of Southern California. Experiments were carried out in a soundproof booth (Acoustic Systems) as described previously (Zhang et al., 2001; Tan et al., 2004; Wu et al., 2006). Female Sprague-Dawley rats (about 3 months old and weighing 250–300 g) were anesthetized with ketamine and xylazine (ketamine, 45 mg/kg; xylazine, 6.4 mg/kg; i.p.). The right auditory cortex was exposed, and the right ear canal was plugged. Multiunit spikes were recorded with parylene-coated tungsten microelectrodes (2 MΩ, FHC) at 500–600 μm below the pial surface. Electrode signals were amplified (Plexon Inc.), band-pass filtered between 300 and 6000 Hz, and then thresholded by custom-made LabView software (National Instrument) to extract the spike times. Pure tones (0.5–64 kHz at 0.1 octave intervals, 25 ms duration, 3 ms ramp) at eight 10 dB spaced sound intensities were delivered through a calibrated free-field speaker facing the left ear. The number of tone-evoked spikes was counted within a window of 10–30 ms from the onset of tone stimulus. The characteristic frequency (CF) of a recording site was defined as the tone frequency at the intensity threshold for spike responses. Auditory cortical mapping was carried out by sequentially recording from an array of cortical sites to identify the location and frequency representation of A1 as previously described. During mapping, the cortical surface was slowly perfused with prewarmed artificial cerebrospinal fluid (ACSF; in mM: NaCl 124, NaH_2PO_4 1.2, KCl 2.5, $NaHCO_3$ 25, glucose 20, $CaCl_2$ 2, $MgCl_2$ 1) to prevent it from drying.

In Vivo Whole-Cell Recording

After premapping of A1, whole-cell recordings (Moore and Nelson, 1998; Margrie et al., 2002; Zhang et al., 2003; Wehr and Zador, 2003; Tan et al., 2004; Wu et al., 2006) were obtained from neurons located at 500–650 μm beneath the cortical surface, corresponding to the input layers of the auditory cortex (Games and Winer, 1988). We prevented cortical pulsation with 4% agarose. For voltage-clamp recording, the patch pipette (4–7 MΩ) contained (in mM) 125 Cs-gluconate, 5 TEA-Cl, 4 MgATP, 0.3 GTP, 10 phosphocreatine, 10 HEPES, 1 EGTA, 2 CsCl, 2 QX-314, pH 7.2, and 0.5% biocytin. Recordings were made with an Axopatch 200B amplifier (Axon Instruments). The whole-cell and pipette capacitance were completely compensated, and the initial series resistance (20–50 MΩ) was compensated for 50%–60% to achieve an effective series resistance of 10–25 MΩ. Signals were filtered at 5 kHz and sampled at 10 kHz. Only neurons with resting membrane potentials lower than −55 mV and stable series resistance were used for further analysis.

To obtain tone-evoked synaptic conductances, the cells were clamped at −70 mV and 0 mV, respectively, which are around the reversal potentials of inhibitory and excitatory currents, as also described in our previous studies (Zhang et al., 2003; Tan et al., 2004; Wu et al., 2006). The linearity of I-V curve (Figure S1) suggests that cortical cells can be reasonably clamped, which is further supported by the fact that when cells were clamped at 0 mV, no significant excitatory currents were observed (Figure 2A), except the outward Cl^- currents. This may be attributed to the use of intracellular cesium, TEA, QX-314, and ketamine anesthesia, which together block most voltage-dependent currents (through K^+ and Na^+ channels and NMDA receptors).

Histological staining of the recorded cells after recording (Horikawa and Armstrong, 1988; Hirsch et al., 2003; Zhu et al., 2004) indicates that the whole-cell voltage-clamp recording method under our current condition sampled pyramidal neurons with a bias. All 25 successfully reconstructed morphologies after whole-cell voltage-clamp recordings showed typical pyramidal cells, consistent with previous work (Moore and Nelson, 1998; Margrie et al., 2002; Wu et al., 2006).

Cell-Attached Recording followed by Current-Clamp Recording or Juxtacellular Labeling

For cell-attached recording, pipettes with smaller tip openings (impedance:10–14 MΩ) were used to overcome the recording bias toward cells with larger cell bodies. Pipettes were filled with ACSF solution containing 0.5% biocytin or intracellular solution containing 0.5% biocytin when subsequent whole-cell current-clamp recordings were to follow. Loose seal (0.2–1 giga Ohm) was made from neurons, allowing spikes only from the patched cell to be recorded. Recording was under voltage-clamp mode without applying a holding voltage. Spike responses are reflected by the current spikes (Figure 4A). Signals were filtered at 0.1–10 kHz. Spike shapes were determined on-line by custom-developed LabView software. The chance of encountering a fast-spike neuron is around 10% in our recording experience. The online spike sorting enabled us to specifically search for fast-spike neurons.

Once the spike TRF was mapped (normally three repetitions), we applied current pulses of 0.25–1 nA for 200 ms ON and 200 ms OFF for up to 20 min (Joshi and Hawken, 2006; Turner et al., 2005; Otmakhova et al., 2002). During and after the protocol, tone-evoked spike responses were monitored to make sure that there was no damage to the cell or drifting of the recording pipette. After the recording, animals were perfused with 4% paraformaldehyde for histological procedures. Normally, juxtacellular labeling only revealed the somatic and dendritic morphologies. Six FS and ten RS cells were successfully reconstructed, and their morphologies are all consistent with that of FS inhibitory neurons and excitatory pyramidal neurons, respectively.

To determine the subthreshold TRFs of fast-spike neurons, the same small-tipped pipettes were used, containing (in mM) 125 K-gluconate, 4 MgATP, 0.3 GTP, 10 phosphocreatine, 10 HEPES, 1 EGTA, 2 QX-314, pH 7.2, and 0.5% biocytin. After identifying the fast-spike cell type and obtaining the complete spike TRF, the cell-attached recording was followed by breaking in the cell membrane. Normal histological procedures were carried out following the current-clamp recording. It should be noted that it remains extremely difficult to achieve high-quality whole-cell recordings under this searching strategy to dissect excitatory and inhibitory synaptic inputs to fast-spike neurons. Nonetheless, the current technique allows us to define the subthreshold and spike response ranges.

Data Analysis

Synaptic Conductances

Excitatory and inhibitory synaptic conductance were derived according to $I(t, V) = G_r(V - E_r) + G_e(t)(V - E_e) + G_i(t)(V - E_i)$. (Borg-Graham et al., 1998; Anderson et al., 2000; Zhang et al., 2003; Wehr and Zador, 2003; Wu et al., 2006). I is the amplitude of synaptic current at any time point; G_r and E_r are the resting conductance and resting membrane potential and were derived from the baseline currents of each recording; G_e and G_i are the excitatory and inhibitory synaptic conductance; V is the holding voltage, and E_e (0 mV) and E_i (−70 mV) are the reversal potentials. In this study, a corrected clamping voltage was used instead of the holding voltage applied (V_h). $V(t)$ is corrected by $V(t) = V_h - Rs \times I(t)$, where Rs was the effective series resistance. A 12 mV junction potential was corrected. By holding the recorded cell at two different voltages, G_e and G_i were calculated from the equation. G_e and G_i reflect the strength of pure excitatory and inhibitory synaptic inputs, respectively. Under holding potentials of –70 mV, activation of NMDA receptors can be ignored (Hestrin et al., 1990; Jahr and Stevens, 1990a, 1990b; Pinault, 1996). Thus, the tone-evoked synaptic currents are primarily mediated by AMPA and $GABA_A$ receptors.

Membrane Potential Responses

Membrane potential was calculated according to $V_{est}(t) = (GrEr + Ge(t)Ee + Gi(t)Ei)/(Gr + Ge(t) + Gi(t))$. V_{est} is the estimated membrane potential change. To estimate the spiking responses of the pyramidal cell from synaptic conductances, the spike threshold is set at 20 mV above the resting membrane potential, according to results from our current-clamp recordings (19.86 ± 4.12 mV, mean ± SD, n = 4). No significant difference in spike threshold was observed

for inhibitory neurons (17.51 and 19.11 mV, n = 2). We noted that by using a different equation with consideration of the cell capacitance (Wehr and Zador, 2003), no qualitative difference in the membrane potential tuning curves was observed. The reversal potential for inhibitory conductance is determined by the ratio of Cl^- concentration in the intrapipette solution and in the cerebrospinal fluid. In our condition, the estimated Cl^- reversal potential is −70 mV after correction of pipette junction potential. In our analyses, we also derived synaptic conductances based on three different presumptive reversal potentials (−60, −70, and −80 mV) and verified that our conclusion was not sensitive to the variation in Cl^- reversal potential.

Frequency Tuning Curves

The Amplitude Envelopes for Excitatory and Inhibitory Inputs. After deriving excitatory and inhibitory conductances at a desired testing intensity, the peak amplitudes of both conductances at each testing frequency were determined. The envelope for peak amplitudes along frequency domain was derived by using a cubic spline interpolation algorithm in the custom-made software in MATLAB.

Normalization of Tuning Curves in Figures 3B and 3E. First, all conductance values in each tuning curve were normalized to the maximum response value. Next, the excitatory tuning curves or the membrane potential tuning curves based on excitation alone were extended or compressed along the frequency axis by a scaling factor to obtain the same half-peak bandwidth (i.e., bandwidth from f_{-50} to f_{50}). These normalized tuning curves were then aligned according to the half-peak bandwidth before averaging. The corresponding inhibitory tuning curve or membrane potential tuning curve based on both excitation and inhibition was normalized by the same scaling factor and was shifted by the same frequency distance.

Tone-Evoked Responses

Spike Responses. With cell-attached recording, spikes can be detected without ambiguity because their amplitudes are normally higher than 100 pA, while the baseline fluctuation is within 10 pA. Tone-driven spikes were identified within a 15 ms time window from a peristimulus-spike-time histogram (PSTH) generated from all the response traces. In anesthetized A1, spontaneous firing in a single cell is lower than 10 Hz, suggesting that the error in defining tone-evoked spikes caused by spontaneous activity is minor. The characteristic frequency (CF) for the spike TRF (either from loose-patch or multiunit extracellular recording) was defined as the logarithmic center of the responding frequency range at the intensity threshold (e.g., Zhang, et al., 2001; 2002).

Synaptic Current and Membrane Potential Responses. These responses were identified according to their onset latencies and peak amplitudes. All the response traces evoked by the same test stimulus were averaged, and the onset latency of this average trace was identified at the time point in the rising phase of response wave form, which was 3-fold of the standard deviation of baseline. Only responses with onset latencies within 7–30 ms from the onset of tone stimulus were considered in this study.

Estimation of CF in Cortical Sites from Premapping

Similar as previously described (Zhang, et al., 2003; Tan et al., 2004), 15 to 20 extracellular recordings were made in each animal to roughly define the tonotopicity of the A1. The CFs of recorded sites were plotted according to the relative cortical coordinates of those sites along the tonotopic axis, and a fitted line was derived to determine a frequency representation gradient (see Zhang et al., 2002). CFs of unrecorded cortical sites in the same A1 were then estimated according to their coordinates in the tonotopic map.

SUPPLEMENTAL DATA

The Supplemental Data for this article can be found online at http://www.neuron.org/cgi/content/full/58/1/132/DC1/.

ACKNOWLEDGMENTS

This work was supported by grants to L.I.Z. from the US National Institutes of Health/National Institute on Deafness and Other Communication Disorders (R03DC006814 and R01DC008983), the Searle Scholar Program, the Klingenstein Foundation, and the David and Lucile Packard Foundation (Packard Fellowships for Science and Engineering).

Received: July 24, 2007
Revised: October 30, 2007
Accepted: January 29, 2008
Published: April 9, 2008

REFERENCES

Agmon, A., and Connors, B.W. (1992). Correlation between intrinsic firing patterns and thalamocortical synaptic responses of neurons in mouse barrel cortex. J. Neurosci. *12*, 319–329.

Anderson, J.S., Carandini, M., and Ferster, D. (2000). Orientation tuning of input conductance, excitation, and inhibition in cat primary visual cortex. J. Neurophysiol. *84*, 909–926.

Azouz, R., Gray, C.M., Nowak, L.G., and McCormick, D.A. (1997). Physiological properties of inhibitory interneurons in cat striate cortex. Cereb. Cortex *7*, 534–545.

Borg-Graham, L.J., Monier, C., and Fregnac, Y. (1998). Visual input evokes transient and strong shunting inhibition in visual cortical neurons. Nature *393*, 369–373.

Calford, M.B., and Semple, M.N. (1995). Monaural inhibition in cat auditory cortex. J. Neurophysiol. *73*, 1876–1891.

Chen, Q.C., and Jen, P.H. (2000). Bicuculline application affects discharge patterns, rate-intensity functions, and frequency tuning characteristics of bat auditory cortical neurons. Hear. Res. *150*, 161–174.

Crook, J.M., Kisvarday, Z.F., and Eysel, U.T. (1997). GABA-induced inactivation of functionally characterized sites in cat striate cortex: effects on orientation tuning and direction selectivity. Vis. Neurosci. *14*, 141–158.

Cruikshank, S.J., Lewis, T.J., and Connors, B.W. (2007). Synaptic basis for intense thalamocortical activation of feedforward inhibitory cells in neocortex. Nat. Neurosci. *10*, 462–468.

Daw, M.I., Ashby, M.C., and Isaac, J.T. (2007). Coordinated developmental recruitment of latent fast spiking interneurons in layer IV barrel cortex. Nat. Neurosci. *10*, 453–461.

Douglas, R.J., and Martin, K.A. (1991). A functional microcircuit for cat visual cortex. J. Physiol. *440*, 735–769.

Games, K.D., and Winer, J.A. (1988). Layer V in rat auditory cortex: projections to the inferior colliculus and contralateral cortex. Hear. Res. *34*, 1–25.

Gibson, J.R., Beierlein, M., and Connors, B.W. (1999). Two networks of electrically coupled inhibitory neurons in neocortex. Nature *402*, 75–79.

Gil, Z., and Amitai, Y. (1996). Properties of convergent thalamocortical and intracortical synaptic potentials in single neurons of neocortex. J. Neurosci. *16*, 6567–6578.

Gonchar, Y., and Burkhalter, A. (1997). Three distinct families of GABAergic neurons in rat visual cortex. Cereb. Cortex *7*, 347–358.

Gupta, A., Wang, Y., and Markram, H. (2000). Organizing principles for a diversity of GABAergic interneurons and synapses in the neocortex. Science *287*, 273–278.

Hendry, S.H., Schwark, H.D., Janes, E.G., and Yan, J. (1987). Numbers and proportions of GABA-immunoreactive neurons in different areas of monkey cerebral cortex. J. Neurosci. *7*, 1503–1519.

Hestrin, S., Nicoll, R.A., Perkel, D.J., and Sah, P. (1990). Analysis of excitatory synaptic action in pyramidal cells using whole-cell recording from rat hippocampal slices. J. Physiol. *422*, 203–225.

Higley, M.J., and Contreras, D. (2006). Balanced excitation and inhibition determine spike timing during frequency adaptation. J. Neurosci. *26*, 448–457.

Hirsch, J.A., Martinez, L.M., Pillai, C., Alonso, J.M., Wang, Q., and Sommer, F.T. (2003). Functionally distinct inhibitory neurons at the first stage of visual cortical processing. Nat. Neurosci. *6*, 1300–1308.

Horikawa, K., and Armstrong, W.E. (1988). A versatile means of intracellular labeling: injection of biocytin and its detection with avidin conjugates. J. Neurosci. Methods *25*, 1–11.

Inoue, T., and Imoto, K. (2006). Feedforward inhibitory connections from multiple thalamic cells to multiple regular-spiking cells in layer 4 of the somatosensory cortex. J. Neurophysiol. *96*, 1746–1754.

Jahr, C.E., and Stevens, C.F. (1990a). A quantitative description of NMDA receptor-channel kinetic behavior. J. Neurosci. *10*, 1830–1837.

Jahr, C.E., and Stevens, C.F. (1990b). Voltage dependence of NMDA-activated macroscopic conductances predicted by single-channel kinetics. J. Neurosci. *10*, 3178–3182.

Joshi, S., and Hawken, M.J. (2006). Loose-patch-juxtacellular recording in vivo-A method for functional characterization and labeling of neurons in macaque V1. J. Neurosci. Methods *156*, 37–49.

Kawaguchi, Y., and Kubota, Y. (1997). GABAergic cell subtypes and their synaptic connections in rat frontal cortex. Cereb. Cortex *7*, 476–486.

Kyriazi, H.T., Carvell, G.E., Brumberg, J.C., and Simons, D.J. (1996). Quantitative effects of GABA and bicuculline methiodide on receptive field properties of neurons in real and simulated whisker barrels. J. Neurophysiol. *75*, 547–560.

Liu, B.H., Wu, G.K., Arbuckle, R., Tao, H.W., and Zhang, L.I. (2007). Defining cortical frequency tuning with recurrent excitatory circuitry. Nat. Neurosci. *10*, 1594–1600.

Margrie, T.W., Brecht, M., and Sakmann, B. (2002). In vivo, low-resistance, whole-cell recordings from neurons in the anaesthetized and awake mammalian brain. Pflugers Arch. *444*, 491–498.

Moore, C.I., and Nelson, S.B. (1998). Spatio-temporal subthreshold receptive fields in the vibrissa representation of rat primary somatosensory cortex. J. Neurophysiol. *80*, 2882–2892.

Mountcastle, V.B., Talbot, W.H., Sakata, H., and Hyvarinen, J. (1969). Cortical neuronal mechanisms in flutter-vibration studied in unanesthetized monkeys. Neuronal periodicity and frequency discrimination. J. Neurophysiol. *32*, 452–484.

Ojima, H., and Murakami, K. (2002). Intracellular characterization of suppressive responses in supragranular pyramidal neurons of cat primary auditory cortex in vivo. Cereb. Cortex *12*, 1079–1091.

Oswald, A.M., Schiff, M.L., and Reyes, A.D. (2006). Synaptic mechanisms underlying auditory processing. Curr. Opin. Neurobiol. *16*, 371–376.

Otmakhova, N.A., Otmakhov, N., and Lisman, J.E. (2002). Pathway-specific properties of AMPA and NMDA-mediated transmission in CA1 hippocampal pyramidal cells. J. Neurosci. *22*, 1199–1207.

Peters, A., and Kara, D.A. (1985). The neuronal composition of area 17 of rat visual cortex. II. The nonpyramidal cells. J. Comp. Neurol. *234*, 242–263.

Pinault, D. (1996). A novel single-cell staining procedure performed in vivo under electrophysiological control: morpho-functional features of juxtacellularly labeled thalamic cells and other central neurons with biocytin or Neurobiotin. J. Neurosci. Methods *65*, 113–136.

Polley, D.B., Read, H.L., Storace, D.A., and Merzenich, M.M. (2007). Multiparametric auditory receptive field organization across five cortical fields in the albino rat. J. Neurophysiol. *97*, 3621–3638.

Priet, J.J., Peterson, B.A., and Winer, J.A. (1994). Morphology and spatial distribution of GABAergic neurons in cat primnary auditory cortex (A1). J. Comp. Neurol. *334*, 349–382.

Shamma, S.A. (1985). Speech processing in the auditory system. II: Lateral inhibition and the central processing of speech evoked activity in the auditory nerve. J. Acoust. Soc. Am. *78*, 1622–1632.

Sillito, A.M. (1977). Inhibitory processes underlying the directional specificity of simple, complex and hypercomplex cells in the cat's visual cortex. J. Physiol. *271*, 699–720.

Sillito, A.M. (1979). Inhibitory mechanisms influencing complex cell orientation selectivity and their modification at high resting discharge levels. J. Physiol. *289*, 33–53.

Simons, D.J., and Carvell, G.E. (1989). Thalamocortical response transformation in the rat vibrissa/barrel system. J. Neurophysiol. *61*, 311–330.

Sohya, K., Kameyama, K., Yanagawa, Y., Obata, K., and Tsumoto, T. (2007). GABAergic neurons are less selective to stimulus orientation than excitatory neurons in layer II/III of visual cortex, as revealed by in vivo functional Ca2+ imaging in transgenic mice. J. Neurosci. *27*, 2145–2149.

Somers, D.C., Nelson, S.B., and Sur, M. (1995). An emergent model of orientation selectivity in cat visual cortical simple cells. J. Neurosci. *15*, 5448–5465.

Suga, N., and Manabe, T. (1982). Neural basis of amplitude-spectrum representation in auditory cortex of the mustached bat. J. Neurophysiol. *47*, 225–255.

Sun, Q.Q., Huguenard, J.R., and Prince, D.A. (2006). Barrel cortex microcircuits: thalamocortical feedforward inhibition in spiny stellate cells is mediated by a small number of fastspiking interneurons. J. Neurosci. *26*, 1219–1230.

Sutter, M.L., and Loftus, W.C. (2003). Excitatory and inhibitory intensity tuning in auditory cortex: evidence for multiple inhibitory mechanisms. J. Neurophysiol. *90*, 2629–2647.

Swadlow, H.A. (1989). Efferent neurons and suspected interneurons in S-1 vibrissa cortex of the awake rabbit: receptive fields and axonal properties. J. Neurophysiol. *62*, 288–308.

Swadlow, H.A. (2003). Fast-spike interneurons and feedforward inhibition in awake sensory neocortex. Cereb. Cortex *13*, 25–32.

Tan, A.Y., Zhang, L.I., Merzenich, M.M., and Schreiner, C.E. (2004). Tone-evoked excitatory and inhibitory synaptic conductances of primary auditory cortex neurons. J. Neurophysiol. *92*, 630–643.

Turner, J.G., Hughes, L.F., and Caspary, D.M. (2005). Divergent response properties of layer-V neurons in rat primary auditory cortex. Hear. Res. *202*, 129–140.

Wang, J., Caspary, D., and Salvi, R.J. (2000). GABA-A antagonist causes dramatic expansion of tuning in primary auditory cortex. Neuroreport *11*, 1137–1140.

Wang, J., McFadden, S.L., Caspary, D., and Salvi, R. (2002). Gammaaminobutyric acid circuits shape response properties of auditory cortex neurons. Brain Res. *944*, 219–231.

Wehr, M., and Zador, A.M. (2003). Balanced inhibition underlies tuning and sharpens spike timing in auditory cortex. Nature *426*, 442–446.

Wu, G.K., Li, P., Tao, H.W., and Zhang, L.I. (2006). Nonmonotonic synaptic excitation and imbalanced inhibition underlying cortical intensity tuning. Neuron *52*, 705–715.

Zhang, L.I., Bao, S., and Merzenich, M.M. (2001). Persistent and specific influences of early acoustic environments on primary auditory cortex. Nat. Neurosci. *4*, 1123–1130.

Zhang, L.I., Bao, S., and Merzenich, M.M. (2002). Disruption of primary auditory cortex by synchronous auditory inputs during a critical period. Proc. Natl. Acad. Sci. USA *99*, 2309–2314.

Zhang, L.I., Tan, A.Y., Schreiner, C.E., and Merzenich, M.M. (2003). Topography and synaptic shaping of direction selectivity in primary auditory cortex. Nature *424*, 201–205.

Zhu, Y., Stornetta, R.L., and Zhu, J.J. (2004). Chandelier cells control excessive cortical excitation: characteristics of whisker-evoked synaptic responses of layer 2/3 nonpyramidal and pyramidal neurons. J. Neurosci. *24*, 5101–5108.